14th IEA Heat Pump Conference
15-18 May 2023, Chicago, Illinois

Transcritical CO_2 heat pump for tap water heating: experimental validation of an auto adaptive algorithm for high pressure optimization

Chiara Corazzol*, Giovanni Rossanese, Sergio Maria Capanelli, Luca Mattiello

CAREL Industries S.p.A., Brugine 35020, Italy

Abstract

Recent developments pushed by F-gas regulations and European guidelines for the renovation of domestic heating systems have led the HVAC market to use new alternatives to propane (R-290) and fluorinated refrigerants. CO_2 (R-744) heat pumps are a consolidated solution for domestic hot water (DHW) applications, with the advantages resulting from using an environmentally friendly, not toxic and not flammable refrigerant. Another benefit of CO_2, when used in DHW applications, is that high-temperature hot water (up to 70°C) can be obtained without the use of a supplementary heating system. In this case, heat rejection pressure has a strong influence on the efficiency of the unit, and there's an optimal value that makes the system reach the maximum coefficient of performance (COP). In this work, the performance of a real transcritical air/water CO_2 heat pump for tap water heating has been investigated and compared at different heat rejection pressure values.
Considering that the optimal pressure value is strictly affected by the variability of the operating conditions (such as water inlet temperature, water outlet temperature or evaporating pressure), an auto adaptive algorithm has been adopted and the consequent results are reported. The algorithm is based on the CO_2 thermodynamic properties calculated via Artificial Neural Network by the controller; one of its main advantages is that it does not require the system modeling and it is not dependent on the use of a specific unit or component.

Keywords: Carbon dioxide, Heat pump, Domestic hot water, Pressure optimization algorithm, Auto-adaptive.

1. Introduction

The crisis due to the conflict in Ukraine and geopolitical instability in general is causing significant repercussions on the European energy market: the uncontrolled increase in gas and electricity prices due to the cut in supplies has led to an increase in costs in various sectors, especially in industrial processes and home heating, markets that have historically relied on gas and other fossil fuels.

Hence the European Union's decision to establish a very aggressive plan for the transition of energy-intensive processes and the technological evolution of systems towards alternatives to gas for residential and industrial applications, focusing the actions above all on the heat pump market: REPowerEU [1] has identified heat pump technology as one of the key technologies for reducing Europe's dependence on fossil fuels in the short and medium term.

In conjunction with these initiatives, which on their own will drive significant market growth, a new proposal has been drafted for the revision of the F-Gas Regulation 517/2014. When the F-Gas Regulation 517/2014 [2] came into force in 2014, it caused a major upheaval in the market, impacting the prices of refrigerants and bringing about the decommissioning of commonly-used refrigerants in the HVAC/R market, to a great extent than if they had actually been banned by law. The proposed revision [3], published on 5 April 2022, aims to introduce further restrictions on the use of HFC and HFO fluids as early as 2024, setting a GWP threshold of 150 for refrigerants used in air conditioning and refrigeration applications. These new limitations, combined with other proposals to ban the use of compounds containing PFAS, chemicals found in many

* Corresponding author. Tel.:+39 049 9731864.
E-mail address: chiara.corazzol@carel.com.

refrigerants currently on the market or the result of their degradation, clearly define the European Union's intention to favour the use of natural refrigerants only in HVAC/R equipment in the near future. The majority of manufacturers have already addressed the use of hydrocarbons, such as propane R-290, as refrigerants in all segments of units intended for the residential air conditioning and heating market. This type of refrigerant has a series of important benefits in terms of operating range, efficiency and design of the units compared to established fluids such as R-410A, as seen in Capanelli [4], yet its high flammability means it is not easily usable in all applications and unit configurations required by the market. CO_2 (R-744) is a natural refrigerant, with GWP=0, and has countless benefits, especially with a view to being used for domestic hot water heating, even if today the main applications are all in the refrigeration market.

It is therefore extremely important to understand and assess the potential of this fluid also in residential applications, so as to define the best combinations of unit design, component selection and process efficiency, and thus make CO_2 a potentially usable option for home air conditioning.

A transcritical unit efficiency can be maximized by correctly managing the working condition. A key-factor on this side is the high pressure of the system which must be tuned in order to get the highest Coefficient of Performance (COP). Liao et al. [5] correlation is extensively used in this field; however in heat pump systems, COP depends also on the secondary fluid capacity, which is a factor not considered in Liao's correlation. An option to improve the high pressure regulation is to use model-based optimization approaches or "ad hoc" correlations, derived from experimental data, such as Zhang et al. [6]. On the other hand, these solutions are often tailored to specific system structures with poor generalization properties. Cervato et al. [7] proposed the use of an Extremum Seeking Control (ESC) that is a real-time optimization approach that does not use a priori model, relying instead on measurements obtained by monitoring the system. Anyway, the COP real-time calculation may result in a burdensome task due to certain limitations and technological constraints typical of industrial scenarios.

To overcome this complications, the present work characterizes the system efficiency by means of a suitable index, defined as simple as possible to be calculated, but accurate enough to guarantee the unit performance. Besides, we use a simple hill climbing algorithm [8], that is an iterative optimization technique.

2. Test Rig Description

Fig. 1 depicts a simplified scheme of the test rig. The unit has two rotary compressors (C_1 and C_2) Toshiba DY45NIFB-10FU with a $45 \cdot 10^{-6}$ m^3 individual displacement. Lubrication is ensured by the oil circuit, which includes an oil separator (SP) and a solenoid valve (SV). A double-wall plate heat exchanger (H) Swep B16DWHx37/3P carries out the heat rejection while a finned-coil evaporator (E) gives the heat load. A receiver (R) is provided to build up a three-pressure levels cycle. The heat rejection and receiver pressures are regulated by V_H and V_R valves respectively, while the evaporating pressure is controlled by the evaporator fan and the superheat at the evaporator outlet is regulated by V_E valve. The secondary fluid for the heat rejection is brine with 16% volumetric concentration of ethylene glycol; the brine circuit includes a variable-speed brine pump (BP) and a volumetric flow meter, measuring the brine flow rate ($\dot{V}_B$).

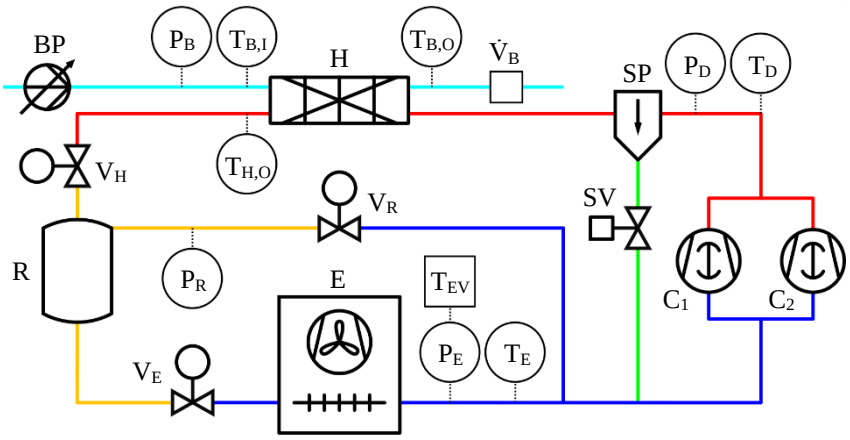

Fig. 1. Transcritical CO_2 heat pump schematic. **B**: brine, **BP**: variable-speed brine pump, **C**: rotary compressor, **D**: discharge, **E**: finned-coil evaporator, **EV**: evaporation, **H**: heat rejection heat exchanger, **I**: inlet, **O**: outlet, **P**: pressure, **R**: receiver, **SP**: oil separator, **SV**: solenoid valve, **T**: temperature, **V**: modulating valve, **$\dot{V}$**: volumetric flow rate.

Temperatures on heat rejection side (T_D and $T_{H,O}$) are measured with ⅒DIN PT100 probes with a 4-wires connection, while on brine side T-type thermocouples are installed ($T_{B,I}$ and $T_{B,O}$). Power consumption of each compressor and its speed-drive is measured by energy meters with ±0.5% of reading accuracy. Brine volumetric flow rate and pressures ranges and accuracies are reported in Table 1.

Table 1. Measuring ranges and accuracies of brine volumetric flow rate and pressures. **RDG**: of reading, **FS**: full scale.

	$\dot{V}_B$ [l h^{-1}]	P_D [barg]	P_B [barg]
Range	40 … 800	0 … 150	-0.5 … 7
Accuracy	± 0.25% RDG	± 1% FS	± 2% FS

All the other variables not described above are gauged by standard industrial sensors.

3. Experimental Tests

The heat pump performance depends on the two fluids capabilities of rejecting and receiving the useful heat load. The unit Coefficient Of Performance (COP) is influenced by the thermodynamic conditions of both CO_2 and brine sides in terms of pressure, temperature and flow rate. For these reasons, a universal correlation able to identify the optimal working point of a particular unit is hard to find, as stated in Fornasieri et al. [9].

The developed algorithm aims to match the two fluid streams through online thermodynamic calculation and simplified modeling of the heat rejection phenomena, without the complication of pure system perturbation as suggested by Cervato et al. [7]. To do so, the measurements on both the heat rejection side (P_D, T_D and $T_{H,O}$) and brine side ($T_{B,I}$ and $T_{B,O}$) are used as inputs of an Artificial Neural Network (ANN) architecture. The ANN has been trained off-line using static data set of CO_2 properties and then implemented inside the unit controller in order to perform the thermodynamic calculations needed.

Assuming that the most stringent constraint is on the brine side, in terms of delivery temperature level, the focus of the present work is dedicated to CO_2 side in terms of heat rejection pressure regulation. During the tests, the discharge pressure P_D has been considered as the independent key-variable to focus on; in fact, the pressure drops recorded across the heat rejection side are comparable with P_D pressure transducer accuracy. The target of the proposed algorithm is then to search for the optimal P_D that maximizes the unit COP, adapting to the imposed brine side conditions.

In the present work, the COP is defined as the ratio between the heat load rejected to the brine side (Q_B) and the electrical power absorbed by the compressors (PWR_C):

$$COP = \frac{Q_B}{PWR_C} = \frac{\dot{V}_B \rho_B c_{P,B} (T_{B,O} - T_{B,I})}{PWR_{C_1} + PWR_{C_2}} \quad [-] \qquad \text{Eq.(1)}$$

Where $\dot{V}_B$ is the brine volumetric flow rate, ρ_B is the brine density and $c_{P,B}$ is the brine specific heat capacity at constant pressure (both calculated using Refprop [10]). Power consumption of the evaporator fan is excluded from the COP calculation, as well as the negligible contributes of variable-speed brine pump and electronics (valves and controls).

The algorithm capability to find the optimal P_D has been tested through different sets of conditions of $T_{B,I}$, $T_{B,O}$ and T_{EV} parameters, while maintaining a 10K constant superheat at the evaporator outlet and a fixed compressors mechanical speed equal to 100rps. Table 2 reports the investigated conditions during the experimental tests.

Table 2. Investigated experimental conditions.

Condition	$T_{B,I}$ [°C]	$T_{B,O}$ [°C]	T_{EV} [°C]
a	15	55 / 65 / 70	-5
b	10	55 / 65 / 70	-5
c	15	55 / 65 / *	-8

* $T_{B,O}$ =70°C not investigated due to system technycal limitations.

$T_{B,I}$ is guaranteed by an auxiliary external chiller, while the brine pump controls $T_{B,O}$. Finally, T_{EV} is controlled at the desired set point by the evaporator fan.

To prove the algorithm quality, the optimal pressure $P_{D,OPT}$ of each investigated condition has been experimentally determined within the transcritical regime $75<P_D<105$barg. To do so, a step-by-step approach has been adopted: for each condition reported in Table 2, P_D has been progressively varied in order to find out the value realizing the maximum COP. Afterwards, the same conditions have been maintained letting the algorithm free to control P_D and converging to a calculated value.

Two indexes are defined for the comparison of the experimental optimal pressure $P_{D,OPT}$ and the algorithm-calculated pressure $P_{D,ALG}$:

$$dev_P = P_{D,OPT} - P_{D,ALG} \ [bar] \quad ; \quad dev_{COP} = \frac{COP_{OPT} - COP_{ALG}}{COP_{OPT}} \cdot 100 \ [\%] \qquad \text{Eq.(2)}$$

These two deviations are considered as representative of the algorithm quality, as they account for both optimal pressure determination accuracy and resulting relative unit performance.

4. Results

Fig. 2(a) reports, by way of example, the experimental curves of Q_B and PWR_C against P_D, while Fig. 2(b) reports T_D and $T_{H,O}$ experimental curves against the same variable. The points resulted by letting the algorithm free to operate in the same conditions are also depicted. The charts are plotted for condition "a" of Table 2 with $T_{B,O}$=55°C.

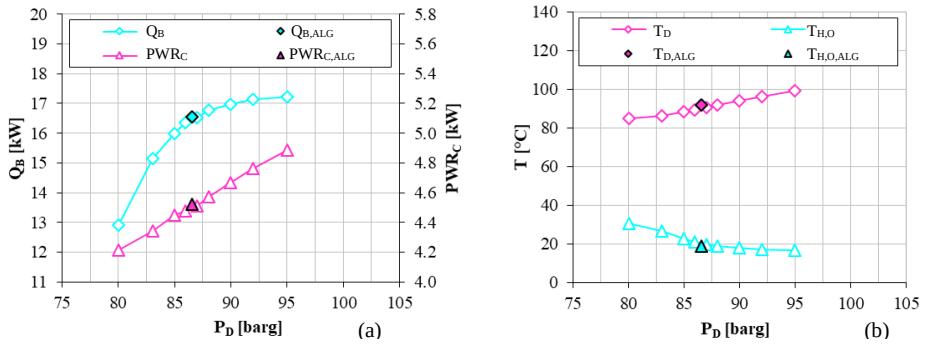

Fig. 2. Condition "a", with $T_{B,O}$=55°C, curves of Q_B, PWR_C (a) and T_D, $T_{H,O}$ (b) with their respective ALG points.

By looking at Fig. 2(a), as expected, both Q_B and PWR_C increase as P_D increases. However, while the first presents a progressively decreasing slope, the second one has a near-linear trend. This justifies the concave shape of the resulting COP curve. It can be also seen that the algorithm is capable of identifying a point where the Q_B curve slope equals the PWR_C curve slope, which is directly related to the optimal point for the heat rejection phenomena. This is also confirmed by Fig. 2(b), as the algorithm point of convergence is close to the change in slope of $T_{H,O}$ curve, i.e. the minimum P_D capable of ensuring a small temperature approach ($T_{H,O}$ - $T_{B,I}$) and an optimized heat rejection. A further increase in P_D, in fact, would have led to a considerable PWR_C increase with a limited increase in Q_B and negligible temperature approach variation.

As additional way of example, the same condition "a" of Table 2 with $T_{B,O}$=55°C is reported in Fig. 3, showing the behavior of the algorithm during a convergence test. It can be seen in Fig. 3(a) an initial pressure set point $P_{D,SET}$ forced to 95barg, then at 00:10 the algorithm is let free to operate. It starts from a value of 88barg, which is the average of condition "a" P_D range, identifying the optimal $P_{D,SET}$. After 10 minutes the algorithm starts to swing around the calculated value of $P_{D,SET}$ close to 86barg and regulates the respective measured pressure $P_{D,MEA}$. The logic correctly reduces $P_{D,SET}$ as the COP increment is visible: from 3.5 to 3.7 as mean values. Correspondingly, Fig. 3(b) shows $T_{B,I}$, $T_{B,O}$ and $\dot{V}_B$ for the same time-frame. It can be seen that $\dot{V}_B$ is correctly regulated by the BP in order to maintain $T_{B,O}$=55°C, so a flow rate reduction is necessary as $P_{D,MEA}$ decreases.

It must be underlined that the BP modulation is completely independent from the algorithm calculation routines. Furthermore, the $P_{D,MEA}$ spike noticeable in Fig. 3(a) at 00:20 (due to an oil refill procedure), does

not destabilize the convergence itself, indicating that the embedded logic is able to bypass harsh disturbances and instabilities.

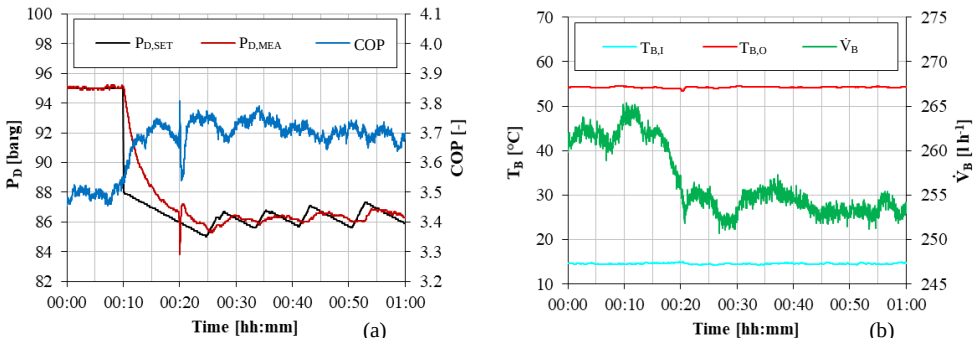

Fig. 3. Condition "a", with $T_{B,O}$=55°C, curves of $P_{D,SET}$, $P_{D,MEA}$ and COP (a) and $T_{B,I}$, $T_{B,O}$ and $\dot{V}_B$ (b).

Fig. 4(a) shows the tests carried out for condition "a", Fig. 4(b) for the condition "b" and Fig. 4(c) for condition "c". Each figure reports the COP trend (Eq.(1)) as a function of P_D for different $T_{B,O}$ ($T_{B,O}$=55°C light blue curve, $T_{B,O}$=65°C green curve and $T_{B,O}$=70°C red curve).

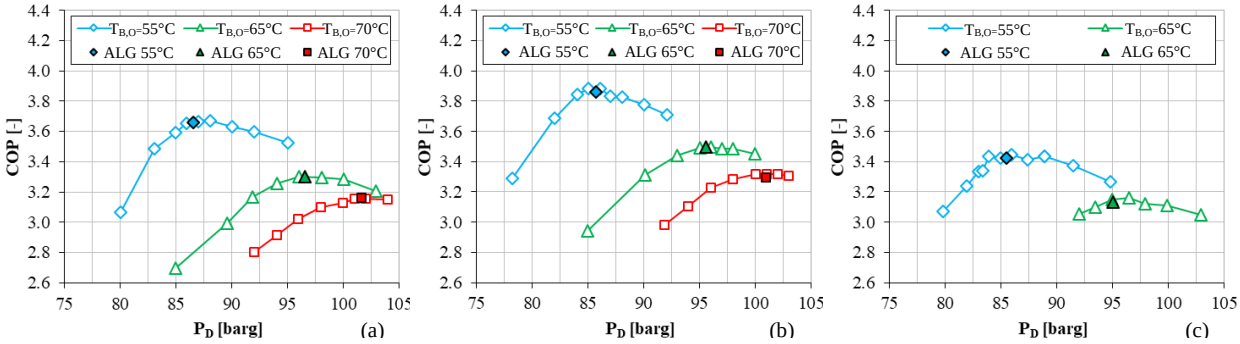

Fig. 4. Experimental COP curves and ALG points for the investigated experimental conditions "a", "b" and "c".

P_D varies within a predefined interval with a higher points density close to the optimal value $P_{D,OPT}$.

As expected, the obtained COP curves are concave functions so that they have a maximum in correspondence of the optimal pressure $P_{D,OPT}$ (i.e. the pressure that allows the best matching of the two fluid streams). For each condition reported in Fig. 4, $P_{D,OPT}$ increases as $T_{B,O}$ increases, causing a consequentially reduction of the COP_{OPT}. As a final step, the auto adaptive algorithm has been tested for the same working conditions: the results are reported in Fig. 4 (solid colour fill markers). It has to be pointed out that the COP_{ALG} reported in the plots are the averages of all the pressure values collected over an observation period of 15 minutes, after the convergence of the algorithm itself.

Results show that the proposed algorithm is capable of converging to a value of COP sufficiently close to the maximum one in all investigated conditions. In fact, dev_{COP} (Eq.(2)) is always less than 1%. Consequently, the resulting discharge pressure $P_{D,ALG}$ is close to the optimal value $P_{D,OPT}$ as $-0.6<dev_P<1.5$bar.

By comparing conditions "a" and "b" it can be noticed that a decreasing in $T_{B,I}$ leads to an increasing of COP_{OPT} for the same $T_{B,O}$ value. This is coherent assuming that the heat rejected is proportional to the brine temperature difference as reported in Eq.(1). Despite the COP_{OPT} values increment, $P_{D,OPT}$ values seems not heavily affected by the different $T_{B,I}$.

By comparing conditions "a" and "c" it can be noticed that a decreasing in T_{EV} causes a decreasing of COP_{OPT} for the same $T_{B,O}$ value. This is coherent assuming that the PWR_C is proportional to compression ratio and this negatively affects the COP value as reported in Eq.(1). Also this comparison shows that $P_{D,OPT}$ values are not heavily affected by the different T_{EV}, even with lower COP_{OPT} values.

Table 3 reports the comparison between the optimal discharge pressures experimentally determined $P_{D,OPT}$ and the ones obtained by the algorithm $P_{D,ALG}$ along with their relatives COP_{OPT} and COP_{ALG}. All the values are referred to the heat load Q_B ranging between 12.9 and 17.8kW.

Table 3. Experimental OPT and ALG pressures P_D and COP with their relative dev_P and dev_{COP} (see Eq.(2)).

Condition	$T_{B,O}$ [°C]	$P_{D,OPT}$ [barg]	$P_{D,ALG}$ [barg]	dev_P [bar]	COP_{OPT} [-]	COP_{ALG} [-]	dev_{COP} [%]
a	55	88.03	86.55	1.48	3.67	3.66	0.27
	65	96.00	96.55	-0.55	3.30	3.30	0.00
	70	102.00	101.61	0.39	3.16	3.16	0.00
b	55	86.06	85.72	0.34	3.88	3.86	0.52
	65	96.00	95.54	0.47	3.50	3.50	0.00
	70	101.02	100.94	0.08	3.32	3.30	0.60
c	55	85.93	85.50	0.43	3.45	3.42	0.87
	65	96.44	95.02	1.42	3.16	3.13	0.95

The values of dev_P are influenced by the arbitrary choice of the pressure values P_D selected to build up the experimental curves in Fig. 4. On the other hand, the values of dev_{COP} are related to the COP resolution chosen (number of significant digits), which justifies the null values appearing in Table 3.

Results indicate that the condition that mostly influences the optimal pressure $P_{D,OPT}$ is the $T_{B,O}$. The variations of $T_{B,I}$ and T_{EV}, have a significant effect in the values of the COP but not a great influence on the optimal pressure determination. The experimental results stated the ability of the proposed auto adaptive algorithm to locate the optimal pressure $P_{D,OPT}$ in all the investigated conditions with a satisfactory approximation.

5. Conclusions

An auto adaptive algorithm for optimal transcritical heat rejection pressure determination has been developed and experimentally investigated on a CO_2 air/water heat pump unit for a Domestic Hot Water (DHW) application. The Artificial Neural Network (ANN) architecture used by the algorithm allows local thermodynamic calculations in order to match the refrigerant and secondary fluid streams so to reach the highest unit Coefficient Of Performance (COP). Experimental tests have been carried out for two levels of evaporating temperature (-5°C and -8°C) and two levels of water inlet temperature (10°C and 15°C) with three values of water outlet temperature (55°C, 65°C and 70°C), maintaining the heat rejection pressure inside the transcritical regime between 75barg and 105barg.

The algorithm showed uniform convergence behavior and robustness against noises and disturbances. Response timings are related to PIDs calibration, which will be considered in future developments.

As expected, the optimal pressure depends on the coupling of CO_2 and water streams capacities. The proposed algorithm is capable of identifying a pressure that matches these two streams, converging on a value close to the optimal one. In fact, the maximum experimental pressure deviation is 1.48bar, resulting in an experimental COP deviation always less than 1% with respect to the maximum. Results show that water outlet temperature is the major factor influencing the optimal pressure, bringing the algorithm to regulate between 85barg and 102barg.

Due to easiness of implementation, a great advantage of such algorithm is the possibility of its inclusion inside an industrial controller with standard computational performances. Furthermore, the absence of a pure system perturbation approach brings significant simplification on its application. Its versatility makes it also suitable for “in situ” direct regulation application as well as laboratory tests on prototype units with the aim of characterization/optimization.

Future works are focused on testing the ability of the algorithm to adapt on different system features such as (but not limited to): fixed-speed water pump with modulating compressors, extended temperature range on water and evaporation sides, heat recovery integrated design, secondary circuit layout coupling.

Nomenclature

Symbols

BP	variable-speed brine pump	[-]	PWR	electrical power	[kW]
C	rotary compressor	[-]	Q	heat load	[kW]
COP	coefficient of performance, Eq.(1)	[-]	R	receiver	[-]
dev	deviation, Eq.(2)	[bar] ; [%]	SP	oil separator	[-]
E	finned-coil evaporator	[-]	SV	solenoid valve	[-]
H	heat rejection heat exchanger	[-]	T	temperature	[°C]
P	pressure	[barg]	V	modulating valve	[-]
PID	Proportional, Integral, Derivative	[-]	$\dot{V}$	volumetric flow rate	[l h^{-1}]

Subscripts

ALG	algorithm-calculated	I	inlet
B	brine	MEA	measured value
C	compressors	O	outlet
D	compressors discharge	OPT	optimal
EV	evaporation	SET	set point value
H	heat rejection		

References

[1] *https://ec.europa.eu/commission/presscorner/detail/en/IP_22_3131* ; Press release.

[2] *https://eur-lex.europa.eu/legal-content/EN/TXT/?uri=CELEX%3A52022PC0150*.

[3] *https://climate.ec.europa.eu/eu-action/fluorinated-greenhouse-gases/eu-legislation-control-f-gases_en*.

[4] Capanelli S.M.; "*Benefits and reliability of air-to-water heat pumps in residential applications, using R-290 refrigerant and an alternative design solution to guarantee high safety with standard components*"; 13th IEA Heat Pump Conference, Jeju, Korea, 2021.

[5] Liao S.M., Zhao T.S., Jakobsen A.; "*A correlation of optimal heat rejection pressures in transcritical carbon dioxide cycles*"; Applied Thermal Engineering 20, pp831-841, 2000.

[6] Zhang X.P., Fan X.W., Wang F.K., Shen H.G.; "*Theoretical and experimental studies on optimum heat rejection pressure for a CO2 heat pump system*"; Applied Thermal Engineering 30, pp2537-2544, 2010.

[7] Cervato A., Corazzol C., Mattiello L., Rampazzo M.; "*Maximizing CO_2 Heat Pump Systems Performance via Extremum Seeking Control*"; 23rd IEEE International Conference on Emerging Technologies and Factory Automation (ETFA), 2018.

[8] Simon D.; "*Evolutionary optimization algorithms*"; John Wiley & Sons, 2013.

[9] Fornasieri E., Girotto S., Minetto S.; "*CO_2 heat pump for domestic hot water*"; 8th IIR Gustav Lorentzen Conference on Natural Working Fluids, Copenhagen, Denmark, 2008.

[10] NIST, "*Refprop Standard Database DLL version 10.0*", Boulder (CO): US Secretary of Commerce, 2018.